Biochemistry

 Volume 19, Number 23 November 11, 1980

Solvent Viscosity and Protein Dynamics†

D. Beece, L. Eisenstein, H. Frauenfelder,* D. Good, M. C. Marden, L. Reinisch, A. H. Reynolds,‡ L. B. Sorensen,§ and K. T. Yue

ABSTRACT: Proteins are dynamic systems. Recent evidence demonstrates that they exist in a large number of conformational substates and can continuously move from one substate to another; motion of a small ligand inside a protein may be possible only through these conformational fluctuations. To test this idea, we study with flash photolysis the binding of CO to protoheme and O_2 and CO to myoglobin in many different solvents. The standard evaluation of such experiments yields information only about the protein–solvent system. A novel approach is presented which permits conclusions concerning the protein: Data from all solvents are considered together, and the rates for transitions of the ligand over various barriers are studied as a function of temperature for fixed solvent viscosities. Results show that over a wide range in viscosity the transition rates in heme–CO are inversely proportional to the solvent viscosity and can consequently be described by the Kramers equation. The rates of O_2 and CO in myoglobin also depend on the solvent viscosity and are most sensitive to the solvent at the lowest viscosity. Viscosity influences protein reactions even in aqueous solutions. The data can be interpreted by a dynamic model in which transitions into and inside myoglobin are governed by fluctuations between conformational substates corresponding to closed and open pathways. Ligand motion thus is mainly controlled by gates and not by static potential barriers. Some characteristic parameters for the substates are determined, and they agree approximately with similar parameters found in Mössbauer experiments. As expected, the barrier parameters evaluated in the novel approach deviate markedly from the ones obtained by the conventional procedure. Comparison with model calculations or basic theories will be meaningful only with the new evaluation, and the method may be essential for many or possibly all biochemical reactions.

Dynamic Barriers in Proteins

A small ligand such as dioxygen (O_2) or carbon monoxide (CO), upon entering or leaving a protein, must overcome barriers. In previous papers (Austin et al., 1975; Alberding et al., 1976, 1978a) we have shown that binding over an extended temperature range, from ~60 to over 300 K, can indeed be described as motion of the ligand over a series of potential barriers, characterized by temperature-independent activation enthalpies and entropies. Below ~200 K, only one binding step is observed, and we interpret it as motion over the final potential barrier at the heme. This transition is not exponential in time and cannot be described by a unique activation enthalpy but can be explained if the protein exists in a large number of conformational substates with slightly different binding rates. Below ~200 K, each protein is frozen into a particular substate with a given activation enthalpy; the rebinding after photodissociation reflects the distribution in barrier heights. At high temperatures, the protein breathes and moves from one conformational substate to another; a ligand that binds sees an average barrier height, and the time dependence should become exponential. Our flash photolysis experiments thus lead to two salient concepts, description of the entire kinetics in terms of a sequence of static potential barriers and conformational substates. The two concepts are, however, incompatible: If the protein fluctuates, the barriers should be dynamic and not static. We are therefore compelled to examine the assumption of static barriers and the evidence for substates in more depth. The existence of conformational substates follows from the general principles of statistical mechanics, and evidence has been seen in many experiments [for a review, see Gurd & Rothgeb (1979)]. Perutz has pointed out that O_2 could not enter or leave Mb[1] if the atoms were fixed in their equilibrium positions (Alberding et al.,

† From the Department of Physics, University of Illinois at Urbana–Champaign, Urbana, Illinois 61801. *Received October 18, 1979.* This work was supported in part by the U.S. Department of Health, Education, and Welfare under Grant GM 18051 and by the National Science Foundation under Grant PCM 79-05072.

‡ Present address: Bell Telephone Laboratories, Murray Hill, NJ 07974.

§ Present address: Division of Applied Sciences, Harvard University, Cambridge, MA 02138.

[1] Abbreviations and symbols used: Mb, ferrous sperm whale myoglobin; G_{ij}^*, H_{ij}^*, and S_{ij}^* denote activation Gibbs energy, enthalpy, and entropy for the transition i → j, with the assumption that protein and solvent together form the complete system; G_{ij}^*, H_{ij}^*, and S_{ij}^* are the corresponding quantities for the protein alone; energies are given in kilojoules per mole; 1 kJ mol^{-1} = 0.239 kcal mol^{-1} = 0.010 eV; entropies are given in terms of the dimensionless ratio S/R, where R = 8.31 J mol^{-1} K^{-1}; CM, carboxymethyl.

0006-2960/80/0419-5147$01.00/0

1978a), Case & Karplus (1979) have demonstrated with trajectory calculations that atoms have to relax in order to let a small ligand escape from the Mb heme pocket (Case & Karplus, 1979; McCammon & Karplus, 1980), and we have seen the spatial distribution of conformational substates in X-ray diffraction (Frauenfelder et al., 1979). Consequently, conformational substates are well established, and we must consider the possibility of a dynamic origin of the barriers. Dynamic theories are rooted in the diffusion model introduced by Kramers (1940); the importance of flexibility for enzyme activity was stressed by Koshland (1958) and others (Weber, 1972; Careri, 1974; Careri et al., 1975). Somogyi & Damjanovich (1975) and Gavish (1978) have suggested that viscosity may play an essential role in determining the dynamic state of the protein through structural fluctuations. [See also Austin & Chan (1978).] In the present paper we discuss experiments on ligand binding after photodissociation in a variety of solvents with different viscosities. We use two approaches to interpret the data. In the first, we treat solvent and protein together, and the binding parameters thus apply to the entire system. In the second, we try to look at the protein only and ask about the influence of the solvent on its dynamic properties. The second approach demonstrates the effect of solvent viscosity on the internal protein barriers and leads to a dynamic model for the protein barriers.

Experimental Approach

We study the binding of CO and O_2 to Mb and protoheme by flash photolysis. The heme system with bound ligand is placed in a cryostat and photodissociated by a flash from a 1-μs dye laser. The subsequent ligand rebinding is followed optically from 2 μs to 1 ks. The apparatus has been described previously (Austin et al., 1975, 1976). The reactions were monitored at 425 nm for protoheme and 436 nm for Mb. A sample cell with an optical path length of 1 cm was used so that the protein concentration (10 μM) could be kept much lower than the free ligand concentration. The 1-μs dye laser pulse had sufficient energy for complete dissociation of CO samples; however, some variance in signal (<5%) occurred for O_2 samples.

Mixtures of water with glycerol, sucrose, ethylene glycol, and methanol were used to vary the solvent viscosity (Curme, 1952; Miner & Dalton, 1953; Douzou, 1977). Since Mb denatures in mixtures of more than 50% methanol, only Mb–O_2 in 50% methanol was analyzed. Phosphate buffer (50 mM), pH 7 in water, was used for the Mb samples. Protoheme was in 1 mM NaOH. Solvents with less than 90% glycerol were equilibrated with 1 atm of CO or air for several hours before being transferred to the cryogenic cell. For the higher viscosity solvents, glycerol was stirred under 1 atm of CO or O_2 for several days. An excess of dithionite, 2:1 for O_2 samples and 10:1 for CO samples, was used for reduction. Since some variation of ligand concentration occurs, the rates for different glycerol–water mixtures were calibrated against measurements at room temperature in cells maintained under 1 atm of CO or O_2.

For the evaluation of second-order rate parameters, values of the solubilities of CO and O_2 in the various solvents are required. Only limited data are available (Seidell, 1940; Ackerman & Berger, 1963), and we therefore determined solubilities by measuring the rate coefficients for the overall binding process Mb + CO $\rightarrow$ Mb–CO and Mb + O_2 $\rightarrow$ Mb–O_2. The first reaction, for instance, satisfies the relation $d[MbCO]/dt = k'[Mb][CO]$. In the limiting cases [Mb] $\gg$ [CO] and [Mb] $\ll$ [CO], the reaction becomes pseudo first order, with rate coefficients $k'[Mb]$ and $k'[CO]$, respectively.

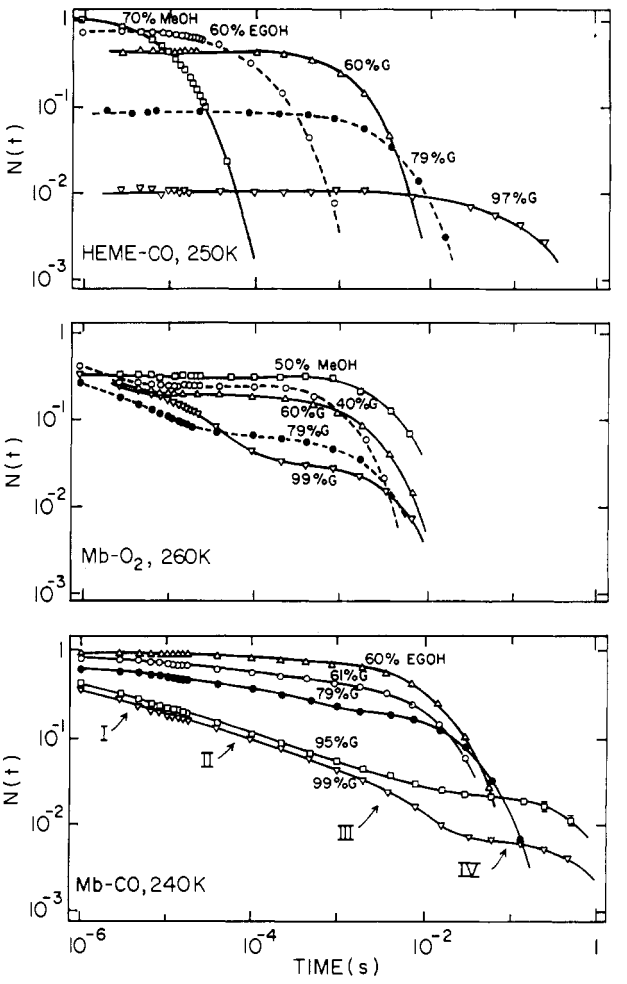

FIGURE 1: Recombination in various solvents at fixed temperature. $N(t)$ is the fraction of heme or Mb molecules that have not rebound a ligand at time t after photodissociation. All Mb–O_2 data shown are for samples equilibrated with air, except the 99% glycerol (1 atm of O_2). G = glycerol (percent by weight), MeOH = methanol (percent by volume), and EGOH = ethylene glycol (percent by weight). Lines are drawn to guide the eye.

We determined the Mb concentrations with a Cary 14 spectrophotometer. The rates measured in the two limiting cases then yield both k' and [CO].

Data

In each experiment we measure the absorbance as a function of time t after photodissociation and compute $N(t)$, the fraction of Mb or protoheme molecules that have not rebound a ligand at time t. Complete sets of curves of log $N(t)$ vs. log t can be found in the earlier papers (Austin et al., 1975; Alberding et al., 1976, 1978a) for one solvent. Here we are interested in the influence of solvent viscosity and show as example in Figure 1 the rebinding curves for heme–CO at 250 K, Mb–O_2 at 260 K, and Mb–CO at 240 K for several different solvents. We have obtained such curves every 10 K between 200 and 330 K. Representative curves below 200 K agree with the data published earlier and show no discernible dependence on solvent.

Data Evaluation

Figure 1 and curves published earlier reveal four processes in the binding of CO to Mb. The approximate positions in time of the four processes are indicated in Figure 1 by the labels I–IV. The rates for I, II, and III are independent of, and IV is proportional to, the ligand concentration in the

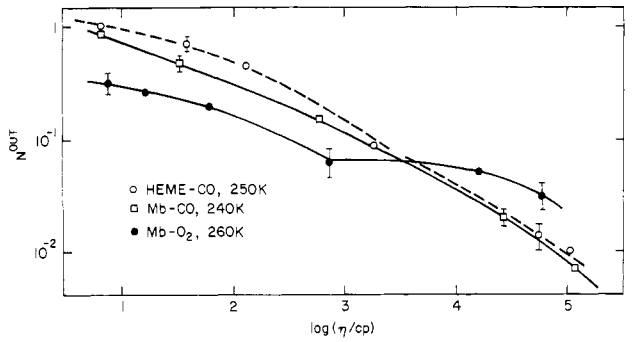

FIGURE 2: N^{out} vs. viscosity at fixed temperature. N^{out} is the fraction of the dissociated ligands that enter the solvent (the normalized amplitude of process IV). Lines are drawn to guide the eye.

solvent after the photoflash. As discussed earlier [particularly in Austin et al. (1975) and Alberding et al., 1978a], in the simplest static model a CO molecule on its path from the solvent S to the binding site A at the heme iron in Mb must overcome four barriers. We describe the binding process by

$$A \underset{k_{BA}}{\overset{k_{AB}}{\rightleftharpoons}} B \underset{k_{CB}}{\overset{k_{BC}}{\rightleftharpoons}} C \underset{k_{DC}}{\overset{k_{CD}}{\rightleftharpoons}} D \underset{k'_{SD}}{\overset{k_{DS}}{\rightleftharpoons}} S$$

where k_{DS}, for instance, denotes the rate coefficient for the transition from D to S. The prime on k'_{SD} denotes a second-order rate. S is the solvent, A the binding site at the heme, and B a state within the heme pocket. C and D are not yet unambiguously assigned, but C may be at the entrance of the heme pocket and D possibly between protein and hydration shell. The step S → D between solvent and protein may be partially diffusion controlled at very high viscosities. The final binding step, B → A, occurs at the heme (Alberding et al., 1978a; Frauenfelder, 1979). The protein barriers B ⇄ C and C ⇄ D have been explored by trajectory calculations (Case & Karplus, 1979). While five states can be seen in Mb–CO, only four appear in Mb–O_2 and three in heme–CO. We call the states in Mb–O_2 A, B, C, and S and in heme–CO A, D, and S.

Before the photoflash, the ligand is bound at the heme iron, state A. The flash breaks the Fe–ligand bond and the ligand moves to B. From there it can either rebind or migrate over the outer barriers. A fraction N^{out} will move all the way into the solvent S; all ligands in the solvent then compete for the vacant binding site and give rise to the concentration proportional process IV. We perform the extraction of the rate coefficients by computer, solving the coupled linear differential equations describing the motion of a particle in four wells (Austin et al., 1975; Frauenfelder, 1978). The procedure yields rate coefficients k_{ij} at each temperature where the process i → j can be seen. The experimental data are accurate enough to determine a single-step reaction rate to ±10%. However, the analysis of multiple-barrier kinetics leads to additional uncertainties in the individual rate coefficients. Parameters for slower processes are influenced by the choice of the rates for the faster processes. An overall error in the rate coefficient of a factor of 2 is estimated, based on the amount parameters could be varied and still fit the data.

Figure 2 shows the fraction N^{out} of ligands that move into the solvent after photodissociation as a function of solvent viscosity at a fixed temperature for Mb–CO, Mb–O_2, and heme–CO. If all barriers were solvent-viscosity independent, then N^{out} would also be independent of solvent viscosity. The fact that N^{out} depends strongly on viscosity implies that at least one of the barriers is influenced by the solvent. Our goal is to understand the solvent influence and find a method to treat the binding process not just in one solvent, but to consider all

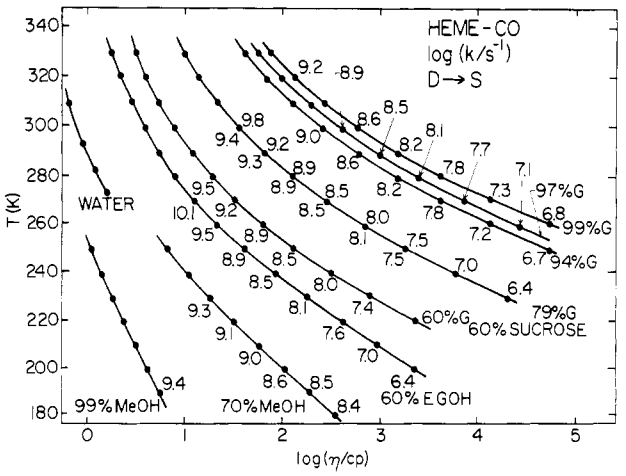

FIGURE 3: The rate coefficient k_{DS} as function of temperature T and viscosity η. The solid lines connect points of the same solvent (G = glycerol, percent by weight; MeOH = methanol, percent by volume; EGOH = ethylene glycol, percent by weight). Values given above points are log k_{DS} for heme–CO. More than 50% MeOH was used for heme only.

solvents together. In order to display the data for a particular transition i → j in all solvents as a function of temperature, we introduce a contour plot as shown in Figure 3 for the step D → S in heme–CO. We characterize a solvent at a temperature T by its viscosity η. The solid lines give the viscosity of a particular solvent as a function of T. In each solvent we have determined the rate coefficient k_{DS} at various temperatures; the resulting values of log k_{DS} are written along the solvent trajectories. Two different solvents can have the same viscosity at a given T and will not a priori yield the same value of log k_{DS}. The experimental data shown in Figure 3 indicate that within errors the value of log k_{DS} is unique. We therefore postulate that log $k_{DS}(T,\eta)$ is a unique and smooth function of T and η. The numbers in Figure 3 characterize the function over a wide range in T and η. The fact that $k(T,\eta)$ is a function of two variables suggests that the set of data in many solvents can be evaluated in more than one way, and we disscuss here two possibilities.

(1) We Consider Protein and Solvent (or Heme and Solvent) Together as One System. In order to evaluate the data for a particular solvent, we parameterize the rate coefficient k_{ij} with the Eyring relation (eq 1). Here, R = 8.31 J mol^{-1} K^{-1} is the gas constant and we take the frequency factor ν to be temperature independent, $\nu = 10^{13}$ s^{-1} for a first-order and $\nu' = 10^{11}$ M^{-1} s^{-1} for a second-order reaction. $G_{ij}^{\ddagger}(T;\text{solv})$ is the activation Gibbs energy and the notation implies that we consider it to be a function of T *for a given solvent.* The decomposition $G^{\ddagger} = H^{\ddagger} - TS^{\ddagger}$ into activation enthalpy $H^{\ddagger}$ and entropy $S^{\ddagger}$ separates the temperature-dependent and temperature-independent component of each transition. From a plot of log $k_{ij}(T;\text{solv})$ vs. $1/T$, we determine $H_{ij}^{\ddagger}$ and $S_{ij}^{\ddagger}$ with eq 1. The procedure just described is the one generally used in the treatment of chemical and biochemical reactions.

$$k_{ij}(T;\text{solv}) = \nu \exp[-G_{ij}^{\ddagger}(T;\text{solv})/RT]$$

$$G_{ij}^{\ddagger} = H_{ij}^{\ddagger} - TS_{ij}^{\ddagger} \qquad (1)$$

(2) We Consider the Protein as the System and Treat the Solvent as External Agent. In this second approach we assume that we can conceptually isolate the protein and investigate how the solvent influences its properties. The correct approach would be to keep all solvent parameters except T constant and measure the rate coefficients k_{ij} as function of temperature. We cannot use this method directly because we do not know

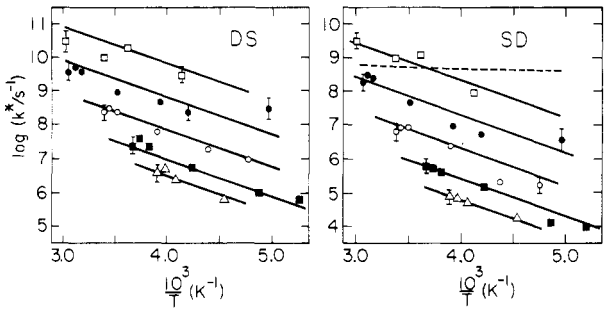

FIGURE 4: Rate coefficients vs. $10^3/T$ at fixed viscosities for heme–CO. Each point on a fixed viscosity curve represents a different solvent. Values of log (η/cP) = 5, 4, 3, 2, and 1 are denoted by Δ, ■, ○, ●, and □. The units for the second-order rate coefficients k_{SD}*′ are M^{-1} s^{-1}. Dotted line is a simple diffusion model: $k_D^o = (8 \times 10^6)RT/3\eta$ with η = 10 cP.

how to determine the relevant variables at the protein surface. We therefore use solvents in which we can vary one property over a wide range and keep the variation of others small. As the crucial variable we select the viscosity η which can be changed over ~5 orders of magnitude. Other properties such as pH, ionic strength, thermal conductivity, and dielectric coefficient vary much less. Even changing the pH from 6 to 10 alters the rate coefficients by less than a factor of 2. At pH 7, the rates are unaffected by a change in the ionic strength from 1 to 200 mM. Moreover, 60% sucrose and 79% glycerol–water, which have the same viscosity but differ in permittivity, show nearly the same rates. Singling out the viscosity as the controlling variable is consistent with the idea that the protein barriers are of dynamic origin and governed by thermal fluctuations (Cooper, 1976). The viscosity of the solvent then determines the time correlation of structural fluctuations (Imry & Gavish, 1974). We consequently assume that the rate coefficients depend on variables other than T only through their dependence on viscosity and write

$$k_{ij}^*(T;\eta) = \nu \exp[-G_{ij}^*(T;\eta)/RT]$$

$$G_{ij}^*(T;\eta) = H_{ij}^*(\eta) - TS_{ij}^*(\eta) \qquad (2)$$

The stars in eq 2 indicate that we are considering the protein alone.[2]

In order to find $k_{ij}^*(T;\eta)$ for constant η, we start from data in the form of Figure 3. Lines of constant η intersect a particular solvent trajectory at a temperature T that can be read from Figure 3; $k_{ij}^*(T;\eta)$ at this temperature is found by interpolating between measured values. As an example, Figure 3 gives log k_{DS}* (238 K; 10^2 cP) = 8.5 for heme–CO. Values of log $k_{ij}^*(T;\eta)$ for heme–CO, Mb–CO, and Mb–O_2 are plotted vs. $1/T$ in Figures 4–6 for five viscosities. If the solvent acts on the protein predominantly through the viscosity, then the barriers should be unaffected by the temperature at a given viscosity. We take this assumption to mean that activation enthalpies H_{ij}* and entropies S_{ij}* depend on viscosity, but not on temperature. The isoviscosity plots of Figures 4–6 are in principle sufficient to determine H_{ij}* and S_{ij}*. In practice, however, the data are not yet accurate enough. We therefore fit the data with models that will be introduced under the

[2] Note that we define $k_{ij}(T,\eta)$ to be a function of the *two* variables T and η; $k_{ij}(T;\text{solv})$ is a function of *one* variable T in a given solvent, and $k_{ij}^*(T;\eta)$ is a function of T at constant solvent viscosity η. Similarly $G_{ij}^*(T;\text{solv})$ describes the transition i → j in a given solvent as a function of the temperature T. $G_{ij}^*(T;\eta)$ characterizes the same transition under the assumption that the protein can be considered separately and the influence of the solvent kept constant by maintaining constant viscosity. In both cases T is the independent variable; solv and η denote the parameters that are kept constant.

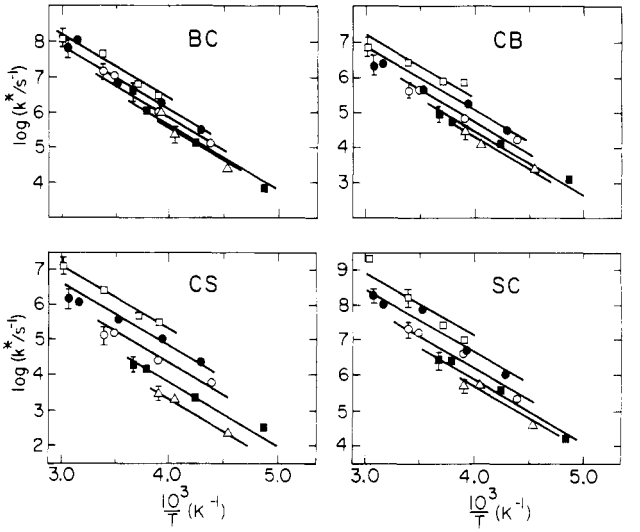

FIGURE 5: Rate coefficients vs. $10^3/T$ at fixed viscosities for Mb–O_2. Symbols are the same as in Figure 4. The units for k_{SC}*′ are M^{-1} s^{-1}.

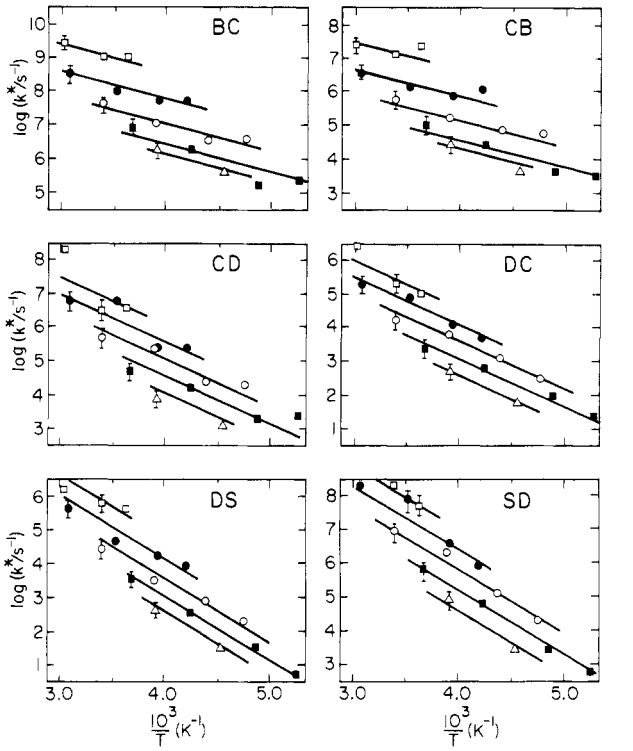

FIGURE 6: Rate coefficients vs. $10^3/T$ at fixed viscosities for Mb–CO. Symbols as in Figure 4. The units for k_{SD}*′ are M^{-1} s^{-1}.

sections Heme–CO and the Kramers Equation and A Dynamic Model. The solid lines in Figures 4–6 are fits to the data based on these models.

With the present experimental apparatus and in the proteins studied so far we have not been able to investigate the influence of viscosity on the innermost barrier B → A at temperatures above 200 K. Since the step B → A is essentially solvent independent below 200 K, we assume that this barrier is not affected by viscosity, and we have used the barrier parameters extrapolated from low-temperature data for the evaluation of the outer barriers.

Discussion

Rate Coefficient Function. In our second approach we consider various solvents and postulate that the influence of

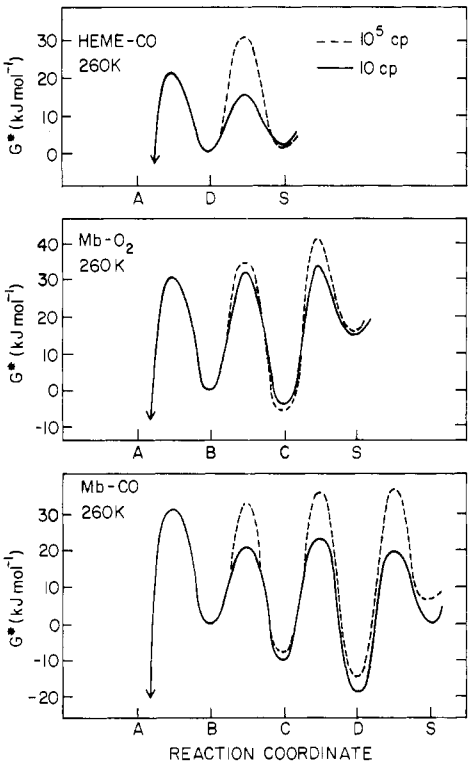

FIGURE 7: The Gibbs energy, G^* (eq 2), at 260 K as a function or reaction coordinate at 10^5 cP (---) and 10 cP (—). A represents the binding site and S the solvent. The Gibbs energies are arbitrarily normalized at well B.

the solvent on the protein occurs predominantly via the solvent viscosity. This viewpoint is supported by Figures 3–6. Figure 3 represents log k_{DS} as a function of T and η. Despite the fact that we have used a variety of solvents, we find that log $k_{DS}(T,\eta)$ is a smooth and unique function of T and η. The curves in Figure 4 correspond to this function at constant values of η, plotted vs. $10^3/T$ instead of T. The curves for the transitions in Mb–O_2 and Mb–CO in Figures 5 and 6 also imply that the rate coefficient is a smooth and single-valued function of T and η. These observations support our postulate that viscosity and temperature together govern the protein dynamics.

Gibbs Energy Barriers. At a given temperature we can express the barrier properties through $G_{ij}^*(T;\eta)$, related to log $k_{ij}^*(T;\eta)$ by eq 2. In Figure 7 we plot the Gibbs energy as function of the reaction coordinate for two extreme values of the solvent viscosity at fixed temperature. We arbitrarily normalize the energy scale to 0 in well B for Mb–O_2 and Mb–CO and in well D for heme–CO. The effect of η on the Gibbs energy differences between the bottoms of adjacent wells is considerably smaller than on the barrier heights. This behavior is in agreement with theory: equilibrium properties are not affected by solvent viscosity, while fluctuations are (Imry & Gavish, 1974).

Viscosity Dependence of Rate Coefficients. In Figure 8 we give the rate coefficients at 260 K for all transitions as a function of viscosity. In heme–CO, the viscosity dependence is strongest. In Mb–O_2, the viscosity dependence decreases as the ligand moves deeper into the protein, and the step B → C is nearly viscosity independent. In Mb–CO all transitions shown depend markedly on log (η/cP). We also plot some values of log k_{ij}^* obtained with Mb–CO in a solidified PVA [poly(vinyl alcohol)] sample (Austin et al., 1975), where the viscosity is very high. An unbiased comparison with the glass samples is not possible because PVA contracts upon drying

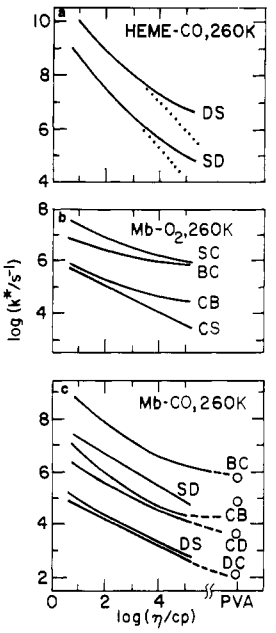

FIGURE 8: Rate coefficients at 260 K vs. log (η/cP). The units for the second-order rate coefficients (S→) are M^{-1} s^{-1}. Values for Mb–CO above the label PVA are for samples in solid poly(vinyl alcohol). The processes DS and SD do not occur for Mb in PVA. Solid lines are calculated from eq 9 (heme–CO) and eq 10 (Mb) with parameters given in Tables II and III. Dotted lines in heme–CO are $1/\eta$ behavior predicted by Kramers equation (eq 8).

Table I: Activation Enthalpies and Entropies for Heme-CO, Mb-O_2, and Mb-CO, Obtained by Using Two Different Approaches[a]

		barrier parameters			
		approach 1, protein plus solvent[b] (79% glycerol)		approach 2, protein at η = 1 P	
system	transition	$H_{ij}^{\ddagger}$/kJ mol^{-1}	$S_{ij}^{\ddagger}/R$	H_{ij}^{*}/kJ mol^{-1}	S_{ij}^{*}/R
heme-CO	D → S	60	16.5	20	−0.2
	S → D	74	24	22	2.3
Mb-O_2	B → C	46	5.4	40	3.3
	C → B	42	0.8	30	−4
	C → S	59	7.8	30	−4.4
	S → C	61	18.6	40	9.0
Mb-CO	B → C	54	11.4	16	−4.3
	C → B	45	3.8	15	−9.2
	C → D	70	16	25	−4.8
	D → C	56	5.7	28	−7.1
	D → S	58	5.3	28	−6.9
	S → D	80	26.2	40	8.7

[a] In approach 1, protein and solvent are considered together, in approach 2 the protein alone is treated as system. Errors are about 10–20%. [b] Some of the numbers for the protein-solvent system differ from the ones quoted in our earlier paper. The new numbers are the result of reanalysis.

and Mb–CO may therefore be under pressure. Nevertheless, the values shown in Figure 8c agree surprisingly well with the high-viscosity extrapolation. The steps D → S and S → D do not occur in PVA samples; the ligand does not leave the protein.

Comparison of the Two Approaches. Both approaches, considering protein plus solvent as system or treating the protein alone, describe all data satisfactorily, but nearly all resulting barrier parameters are significantly different. In Table I we compare values of the activation enthalpies and entropies deduced by the two approaches with eq 1 and 2.

Differences are striking. The description in terms of the protein–solvent system leads to large activation enthalpies and entropies. Values for the protein alone are lower, the preexponential factor approaches the value of 10^{13} s^{-1} expected from naive arguments, and the activation entropies are close to zero.

To establish the connection between these two approaches, we note that the Gibbs activation energy at a given temperature for a particular solvent–protein system can be written in two ways:

$$G^{\ddagger}(T;\text{solv}) \equiv H^{\ddagger} - TS^{\ddagger} = H^{*}[\eta(T)] - TS^{*}[\eta(T)] \quad (3)$$

$H^{\ddagger}$ and $S^{\ddagger}$ are assumed to be temperature independent and $\eta(T)$ is the solvent viscosity at temperature T. We further assume that the solvent viscosity is governed by an Arrhenius law,[3] $\eta(T) = \eta_0 \exp(E_\eta/RT)$, and that over a wide range in viscosity $H^{*}(\eta)$ and $S^{*}(\eta)$ depend linearly on ln η

$$H^{*}[\eta(T)] \cong H^{*}(0) + h \ln \eta(T)$$

$$S^{*}[\eta(T)] \cong S^{*}(0) + s \ln \eta(T) \quad (4)$$

We will justify eq 4 under A Dynamic Model. Inserting these expressions into eq 3, using the approximation $1/T \cong (2/T_0) - (T/T_0^2)$ where T_0 is an average temperature, and equating coefficients of equal powers of T yield

$$H^{\ddagger} = H^{*}[\eta(T_0)] + E_\eta\left(\frac{h}{RT_0} - \frac{s}{R}\right)$$

$$S^{\ddagger} = S^{*}[\eta(T_0)] + \frac{E_\eta}{T_0}\left(\frac{h}{RT_0} - \frac{s}{R}\right) \quad (5)$$

The activation enthalpy $H^{\ddagger}$ for the protein–solvent system differs from the average "intrinsic" activation enthalpy $H^{*}[\eta(T_0)]$ by a term that contains the activation energy E_η for the solvent viscosity and the viscosity dependences of $H^{*}(\eta)$ *and* $S^{*}(\eta)$. A similar term occurs in the difference between $S^{\ddagger}$ and $S^{*}[\eta(T_0)]$.

Comparison with Model Calculations. One goal of kinetic studies is a set of barrier parameters that can be compared with model calculations. The results of the present paper, particularly those under Comparison of the Two Approaches, imply that such a comparison is meaningful only if the effect of the solvent on the protein is taken into account. Theory and experiment may be matched most easily in two limiting cases. The *high-viscosity limit* is the first case. Figure 8 suggests that log $k_{ij}^{*}(T;\eta)$ tends toward a limit as $\eta \to \infty$. This situation may be modeled by assuming that the protein surface is fixed and the residues that reach into the solvent matrix are immobilized in specific substates. The *low-viscosity limit* is the second case. It may be possible to model the limit $\eta \to 0$ by assuming that residues on the surface move unhindered and that the protein breathes and fluctuates freely. Figure 8 implies, however, that the low-viscosity plateau has not been reached at 10 cP and many of the rate coefficients assume their largest slope at the smallest viscosity studied. This behavior can be understood: Consider a sphere of mass m and radius R on a spring, oscillating with angular frequency ω. If placed in a medium with viscosity η, the motion will be damped by the Stokes force $6\pi\eta v_0 R$, where v_0 is the velocity. The motion becomes aperiodic if $6\pi\eta R = 2m\omega$ or if $\eta = (m/R)(\omega/3\pi)$. $(m/R) = \rho$ is a linear mass density (mass per unit length). The motion is therefore aperiodic if the viscosity satisfies the relation

$$\eta_{\text{crit}} = \rho\omega/3\pi \quad (6)$$

The motion is overdamped if $\eta > \eta_{\text{crit}}$ and underdamped if $\eta < \eta_{\text{crit}}$. The two limiting cases treated above can now be defined by

$$\eta \gg \eta_{\text{crit}} \text{ (system frozen)}$$

$$\eta \ll \eta_{\text{crit}} \text{ (system free)} \quad (7)$$

The criterion (eq 7) cannot be applied in a straightforward way to protein reactions, because the viscosity of the solvent and the protein can be vastly different. As a simple model, to be discussed in more detail under A Dynamic Model, we take the situation where the ligand moves inside the protein, but the motion is affected by the protein dynamics which, in turn, is governed by the solvent viscosity η. In the simplest case the dynamics may be controlled by the motion of a residue that sticks into the solvent and can either be immobilized in various substates in a highly viscous solvent ($\eta \to \infty$) or move freely in vacuum ($\eta \to 0$). For such a residue, the linear mass density is on the order of 10^{-14} g cm^{-1} and $\omega/3\pi$ ranges from below 10^{11} to 10^{14} s^{-1} (McCammon & Karplus, 1980), leading to critical viscosities between 1 mP and 1 P. The limit of high viscosities should consequently be reached at ~10 P. The data in Figure 8 indicate that the high-viscosity plateau is only reached at or above 10^3 P; the effective viscosities consequently may be smaller than the static solvent viscosity.

Equation 6 implies that the low-viscosity plateau should occur well below 1 cP. Since actual vibrational motions in proteins could extend below values of $\omega/3\pi$ of 10^{11} s^{-1}, the limit may even be lower. Indeed, the curves in Figure 8 reach their largest slope at ~10 cP, and no evidence for a low-viscosity plateau is visible. Since water has a viscosity of 1 cP at 300 K, proteins are not in the low-viscosity regime even in aqueous solutions.

While comparison between theory and experiment may be most easily achieved for $\eta \to 0$ and $\eta \to \infty$, the general case is more important for protein dynamics. If fluctuations in the solvent act as driving forces for protein reactions and catalysis, then calculations at a realistic viscosity, taking into account the motion of the protein surface, are desirable.

Heme–CO and the Kramers Equation

In an earlier publication (Alberding et al., 1976), we have introduced a model for the binding of CO to heme in which S is the solvent and D a cage close to the heme iron. The transition S → D is a second-order reaction in which a CO molecule in the solvent moves into the cage; D → S is the inverse step in which a CO molecule leaves the cage.

The data in Figure 8a indicate that for viscosities between about 10 and 10^3 cP the rates $k_{SD}^{*\prime}$ and k_{DS}^{*} are inversely proportional to the viscosity η. Above ~10^3 cP, both rate coefficients deviate from this proportionality. The η^{-1} dependence suggests that the transitions S → D and D → S can be described by Kramers' theory (Kramers, 1940; Chandrasekhar, 1943; Brinkman, 1956; Skinner & Wolynes, 1978). Kramers assumed that the shuttling action of Brownian motion allows a particle to escape over a potential barrier, and he obtained for the rate coefficient

$$k^{*} = \frac{\nu_0\nu_0'\rho}{3\eta} e^{-H^{*}/RT} \quad (8)$$

Here ν_0 is the undamped frequency in the initial well, ν_0' the corresponding frequency at the top of the inverted barrier, ρ

[3] In reality, $\eta(T)$ does not follow an Arrhenius law, but the deviations do not affect the considerations given here.

Table II: Barrier Parameters for Heme-CO[a]

transition	H^*/kJ mol^{-1}	$\nu_0\nu_0'$	log A^0
D → S	20	2.4 × 10^{27} s^{-2}	10.7
S → D	22	3.0 × 10^{26} s^{-2} M^{-1}	9.2

[a] The parameters are obtained by fitting eq 9 to the experimental data and using $\rho = 10^{-14}$ g cm^{-1}.

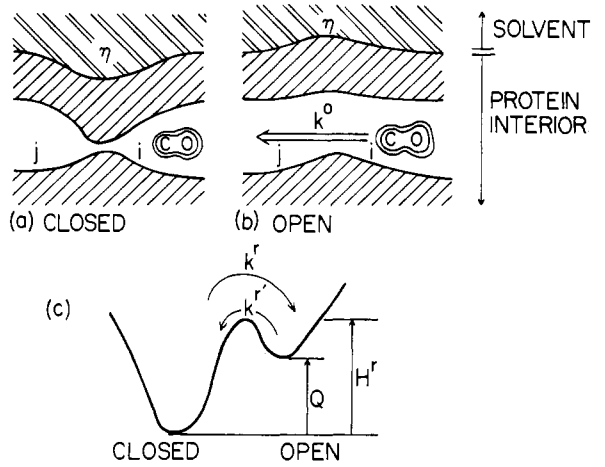

FIGURE 9: A CO molecule inside Mb moves from state i to j. In (a) Mb is in a conformational substate where the channel from i to j is closed, and in (b) the gate is open. (c) gives the potential for conformational transitions between the open and the closed substates.

the linear mass density, and H^* the barrier height. Equation 8 fits the data well to ~10 P. To describe the deviation at high viscosities, we add a viscosity-independent term to eq 8:

$$k^* = \left(\frac{\nu_0\nu_0'\rho}{3\eta} + A^0\right)e^{-H^*/RT} \qquad (9)$$

Equation 9 fits the data for CO binding to heme very well; the fits are shown as solid lines in Figures 4 and 8 and the resulting values of $\nu_0\nu_0'$, A^0, and H^* are listed in Table II. Under Summary we discuss the use of the Kramers equation instead of the more familiar transition state eq 1.

The deviation from the simple Kramers behavior above ~10 P is not unexpected. Equation 8 is based on Stokesian motion. At high frequencies, the motion becomes non-Stokesian (McCammon & Wolynes, 1977). More work is required to learn if this behavior can lead to the observed deviations.

A Dynamic Model

If proteins were rigid, the solvent viscosity η would not affect interior transitions. The viscosity dependences exhibited in Figures 5 and 6 thus imply a dynamic origin of the interior barriers. Indeed, as already pointed out in the introduction, Case & Karplus (1979) have shown that interior groups must move in order to let a small ligand escape from the heme pocket. Their calculation suggests a simple dynamic model that may explain how the solvent viscosity can affect the barriers inside a protein. Two features that such a model must describe are contained in Figures 4–6. First, over a wide range in η, log k_{ij}^* is approximately proportional to log η; k_{ij}^* consequently is proportional to a power of η, $k_{ij}^* \propto \eta^{-\kappa_{ij}}$. Second, for some transitions k_{ij}^* tends toward a limiting value at high viscosities. The proposed model is shown in Figure 9. We consider the motion of a CO molecule inside Mb from state i to j. Mb is assumed to have two conformational substates, "open" and "closed". In the open state, the transition from i to j is given by the rate coefficient k^o, in the closed state it cannot occur. With k^r, we denote the relaxation rate coefficient for the transition from the closed to the open substate; $k^{r\prime}$ is the coefficient for the reverse step. Parts a and b of Figure 9 represent the real states i and j inside the protein, and Figure 9c depicts the open and closed conformational substates. For simplicity we assume $k^r \ll k^{r\prime}$ and $k^o \gg k^{r\prime}$. The first assumption implies that the probability of finding the system in the open state is small, the second that the transition i → j in the open state is fast compared to closing of the passage. Both restrictions can easily be relaxed if necessary. With these assumptions, the transition of a CO molecule from i to j is given by $k_{ij}^* \cong k_{ij}^r$.

Table III: Parameters Resulting from a Fit of Equations 10 and 11 to $k_{ij}^*(T;\eta)$

		barrier parameters			
system	transition	log A_{ij}[a]	log A_{ij}^0[b]	κ	H^r/kJ mol^{-1}
Mb-O_2	B → C	14.1	12.8	0.4	35
	C → B	13.1	11.4		
	C → S	13.1	(<10.5)	0.5	35
	S → C	14.9	12.9		
Mb-CO	B → C	12.5	9.1	0.8	15
	C → B	10.6	7.4		
	C → D	12.2	(<8.5)	0.5	27
	D → C	10.7	(<8.0)		
	D → S	12.8	9.7	0.6	36
	S → D	15.1	(<12)		

[a] Units for A_{ij} are, for the transitions from well S, s^{-1} M^{-1} cP$^{\kappa}$ and for all other transitions s^{-1} cP$^{\kappa}$, where cP = centipoise = 10^{-2} g cm^{-1} s^{-1}. [b] Units for A_{ij}^0 are, for the transitions from well S, s^{-1} M^{-1} and for all other transitions s^{-1}.

To fit the experimental data, we use eq 9 as guide and write

$$k_{ij}^*(T;\eta) = \left(\frac{A_{ij}}{\eta^{\kappa_{ij}}} + A_{ij}^0\right)\exp(-H_{ij}^r/RT) \qquad (10)$$

This expression contains the power-law dependence and the limiting high-viscosity rate. The first term in the parentheses, $A_{ij}/\eta^{\kappa_{ij}}$, describes the interaction of the protein with the solvent. Analogy to the Kramers expression suggests that it is caused by the shuttling action of the Brownian motion in the solvent but attenuated and transformed by the protein. The meaning of the second term, A_{ij}^0, is ambiguous. The Mb–CO results in Figure 8 demonstrate that even with rigid protein surroundings (PVA) the interior rates do not vanish. Some internal motion may survive and open the gate. Alternatively some ligands may pass from i to j even in the closed substate. We tentatively favor the first explanation because the activation enthalpies for both terms in the parentheses in eq 9 appear to be the same.

The model of Figure 9 implies that a transition i → j and its inverse j → i are governed by the same internal gate and relaxation process. In fact, a fit of eq 10 to the data gives $H_{ij}^r \approx H_{ji}^r$ and $\kappa_{ij} \approx \kappa_{ji}$. In order to restrict the number of free parameters, we therefore assume for the data evaluation that

$$H_{ij}^r = H_{ji}^r \qquad \kappa_{ij} = \kappa_{ji} \qquad (11)$$

The experimental data shown in Figures 5 and 6 at all temperatures and viscosities can be fitted with eq 10 and 11. The resulting parameters are listed in Table III, and the fits are shown as solid lines in Figures 5 and 6.

The model of Figure 9 reproduces the data over a wide range in temperature and viscosity surprisingly well even though we used the simplest assumptions. It is likely that more than two conformational substates exist. The open transition parameter k^o may be comparable to k^r and may be different in the two

directions. Such generalizations can be taken into account if the data warrant it. Since we can fit all data for a given barrier i $\rightleftarrows$ j with six parameters, A_{ij}, A_{ji}, A_{ij}^0, A_{ji}^0, H^r, and κ, there is no need yet for a generalization. More important are theoretical investigations to explain the observed features such as the power-law dependence on viscosity.

The model of Figure 9 is symmetric under the exchange i $\leftrightarrow$ j; together with the assumption $k^o \gg k^{r\prime}$, this symmetry implies that ligands move with equal rate either way: $k_{ij}^* = k_{ji}^*$. Indeed, the data show that this prediction is correct in a first approximation, and eq 11 expresses part of the equality. A closer look, however, shows deviations from the equality, and these are expressed in Table III by $A_{ij} \neq A_{ji}$. The interaction of the ligand with the protein provides a plausible explanation for the symmetry violation. If the ligand influences the protein motion differently in state i than in state j or if the entropy of the protein–ligand system is different in the two states, then we expect $A_{ij} \neq A_{ji}$. Independent evidence for the effect of the ligand on the protein comes from a comparison of the data for Mb–CO and Mb–O_2. If the protein were not affected by the ligand, then we would expect a closer similarity. Table III shows that the outermost barrier is essentially identical for Mb–CO and Mb–O_2, but the inner ones are distinctly different. Moreover, Mb–CO shows four barriers, and Mb–O_2 shows only three.

According to the general ideas underlying the model of Figure 9, the relaxation enthalpy H^r depends on the specific part of the protein involved in a particular transition i $\leftrightarrow$ j, and Table III suggests a value of $\sim$35 kJ mol^{-1} for some of the main transitions. An investigation of relaxation rates by the Mössbauer effect (Parak et al., 1980; Keller & Debrunner, 1980) yields a similar value for H^r. The close agreement may be fortuitous because the Mössbauer experiments are performed with metmyoglobin and measure the relaxation at the heme iron, while our studies refer to ferrous Mb–O_2 and Mb–CO and look at barriers that may be some distance from the heme group.

A final remark in this section concerns eq 4. The observed dependence $k^* \propto \eta^{-\kappa}$, together with eq 2, justifies eq 4.

Summary

In the present paper we imply that much of the work on biochemical kinetics has to be reinterpreted, data evaluation should be performed in a novel way, transition state theory is not adequate, and barriers are dynamic, not static. Since these claims are certain to be questioned, we summarize here the steps that lead to these claims, review the assumptions, add further support, and discuss some consequences.

Why a New Approach? Proteins are now known to exist in many conformational substates and to fluctuate rapidly from one substate to another. The potential barriers observed in the migration of a ligand inside a protein can in general therefore not be independent of temperature and solvent properties. In order to explore the dynamic features of the barriers, we evaluate our flash photolysis experiments in two ways, either by treating protein plus solvent as system or considering the protein alone (see Data Evaluation). The second approach requires that protein reactions be studied over wide ranges in temperature and solvent viscosity. If the protein were a static and rigid entity, the two approaches would yield identical results. The fact that activation enthalpies and entropies extracted by the different routes are in general vastly different (Table I) verifies that the protein is a dynamic system and influenced by the solvent.

The Crucial Assumptions. The material discussed under Data Evaluation is based on three assumptions: (1) The migration of the ligand from the solvent to the binding site in myoglobin involves three successive barriers for oxygen and four for carbon monoxide. (2) The innermost barrier, controlling the ligand binding at the heme group, operates at all temperatures; the relevant barrier parameters, determined between 60 and 160 K, are viscosity independent and can be extrapolated to 300 K. (3) Because the protein is not a rigid system, solvent properties affect the barriers inside the protein. The dominant solvent parameter is the viscosity; other parameters such as pH, ionic strength, and permittivity can be neglected in a first approximation. Consequently, we can consider a particular transition i $\rightarrow$ j in many different solvents and describe it by the rate coefficient $k_{ij}(T;\eta)$. In the following three sections, we justify the three assumptions.

Multiple Barriers. We have justified assumption 1 in a previous paper (Austin et al., 1975, in particular, subsections 6.3 and 10.1). We will not repeat the discussion here but note that the multiple-barrier model quantitatively describes the data in the temperature range from 40 to 300 K and the time range from 1 μs to a few ks. Moreover, Sharrock & Yonetani (1980) have performed CO-binding experiments on heme-substituted myoglobins and have been able to fit their data quantitatively with a four-barrier model. In order to eliminate the possibility that different myoglobin components give rise to the different processes, we have also studied the principal component separated by CM-cellulose cation-exchange chromatography and see no difference. Finally, Case & Karplus (1979) find with trajectory calculations that the path from the heme pocket to the protein surface involves multiple barriers.

The most convincing feature of a model is, however, not the ability to describe a known set of data, but its predictive power. Two predictions of our model are verified by experiments, the binding kinetics with mixed ligands (Beece et al., 1979) and the speedup of the internal process III at high ligand concentration (Alberding et al., 1978b). At ligand pressures above $\sim$1 MPa (10 bar), states within the protein become multiply occupied, the linear deterministic rate equations normally used become invalid, and the internal process III begins to speed up.

Despite the success of the sequential model, other choices cannot be ruled out entirely. Branched models will also fit the data, but only the sequential model results in eq 11, $H_{ij} = H_{ji}$ and $\kappa_{ij} = \kappa_{ji}$. The sequential model therefore describes the entire data set with the smallest number of parameters. Even in branched models, the general features of the viscosity dependence are retained.

Innermost Barrier. The last step in ligand binding, B $\rightarrow$ A, occurs in the heme pocket. We have studied this process in detail at temperatures below 200 K (Austin et al., 1975; Alben et al., 1980). The low-temperature data can be fit by a temperature independent distribution of activation enthalpies. The rate coefficients k_{ij} for transitions other than B $\rightarrow$ A are computed by assuming that the barrier between B and A is present at all temperatures. k_{BA} above $\sim$200 K is given by the full distribution for times less than a certain relaxation time and the average rate of the distribution for longer times. Evidence for the validity of this assumption comes from nanosecond flash photolysis experiments on Hb–CO and Hb–O_2 (Alpert et al., 1974, 1979) at $\sim$300 K in which process I is clearly observable. We have also seen process I at 300 K in Mb–O_2 with a nanosecond laser system. The presence of process I at 300 K with about the correct lifetime further strengthens the multibarrier model. It is possible that protein relaxation renders the transition B $\rightarrow$ A above $\sim$200 K somewhat faster than predicted by straightforward extrapo-

lation. Such a speedup would alter some the numbers in Tables II and III but would not affect our model and our conclusions.

Solvent Viscosity as Dominant Factor. Assumption 3 that the rate coefficients $k_{ij}(T,\eta)$ for ligand transitions inside Mb depend only on the temperature T and the solvent viscosity η is the essential new element in our approach and permits treating the data from many solvents together in a unified way. Support comes from three observations: (a) The coefficient $k_{DS}(T,\eta)$ for heme–CO shown in Figure 3 is a smooth function of T and η. If the solvents affected the transition D → S through parameters other than T and η, discontinuities would appear. The same argument for all other transitions is made by the data in Figure 4 for heme–CO and Figures 5 and 6 for Mb–O_2 and Mb–CO. The constant viscosity cuts in these figures are smooth functions of T at all viscosities, showing that the $k_{ij}(T,\eta)$ are indeed functions of T and η only. (b) Variations in pH, ionic strength, and permittivity affect the rebinding kinetics very weakly. (c) Some solvents partially unfold Hb (Hershkovits et al., 1970) and could consequently change the binding processes. We have measured the optical spectrum in each solvent and only used systems that showed no evidence for unfolding.

Myoglobin, of course, is a particularly simple protein, known to be largely insensitive to parameters such as pH. This insensitivity permits us to consider the rates to be functions of T and η only. In proteins other than myoglobin additional factors such as pH are influential. For extraction of the viscosity effect, such parameters must be kept constant while viscosity and temperature are varied. Even in a pH-sensitive system such as bacteriorhodopsin, we have, however, found the viscosity dependence to be important (Beece et al., 1980).

Model Dependence. At this point we can state with some confidence which of our conclusions depend critically on the assumptions listed under The Crucial Assumptions. The observation that solvent viscosity strongly affects protein function is independent of all assumptions. The isoviscosity approach treated under Data Evaluation is independent of assumptions 1 and 2. The detailed values given in Tables I and II are based on assumptions 1–3. A major change in the reaction scheme would probably lead to rather different numbers. A minor change, for instance the addition of some small-probability parallel pathway, would change the parameters only by the corresponding small fraction.

Kramers Equation. The fitting of our data by modified Kramers equations, eq 9 and 10, calls for some comments. We initially planned to use the customary transition state relation, eq 1. However, our results as shown in Figures 4–8 clearly express the fact that the rate coefficients at constant T depend on viscosity and that eq 1 therefore is inadequate. Indeed, Kramers already pointed out in his pioneering work (Kramers, 1940) that conventional transition-state theory is valid, at best, in a limited region of damping (viscosity). Later theoretical work (Hill, 1976; Skinner & Wolynes, 1978; Montgomery et al., 1979) has verified this limitation. A necessary but not sufficient condition for the applicability of transition state theory is

$$\eta < \eta_{crit} \tag{12}$$

where η_{crit} is defined in eq 6. Since η_{crit} can be as small as 1 mP, the validity of transition-state theory is doubtful even in aqueous solutions. Indeed, our results imply a strong viscosity dependence of the rate coefficients already at the lowest viscosities studied (Figure 8). Evidence for the importance of the Kramers relation eq 8 had already been found earlier in polymer studies (Bullock et al., 1974) and enzyme reactions (Gavish & Werber, 1979). The use of the Kramers relation (eq 1) consequently is based on sound theoretical and experimental information.

In eq 9, we have added a second term to eq 8. This term describes the observation that deviations from eq 8 must occur at very high viscosities; otherwise, no reactions would occur in solids. An understanding of the term will require more theoretical work.

In eq 10, we have modified the Kramers relation by replacing η by η^κ. This modification, forced on us by the experiments, describes the fact that η is the solvent viscosity but that the transitions take place inside the protein. The effect of the solvent viscosity therefore is shielded and attenuated; the coefficient κ characterizes this shielding. A discussion of this point is given by Gavish (1980).

Kramers originally derived eq 8 for a one-dimensional barrier. The generalization to three dimensions (Brinkman, 1956; Landauer & Swanson, 1961; Larson & Kostin, 1978) shows that the preexponentials A_{ij} and A_{ij}^0 in eq 10 contain an entropy factor, $\exp(S^*/R)$. Kramers' theory and most of the later work are based on classical physics. A recent paper (Ishioka, 1980) treats the problem quantum mechanically; the fundamental results remain unchanged, but tunneling is automatically taken into account.

Dynamic Model. In the simplest terms, a barrier governing the transition between two states can be described by two extreme models, a stationary potential barrier or a gate that opens and closes. In our earlier papers (Austin et al., 1975) we have used stationary potential barriers; in the present paper we switch to the dynamic picture. Reality lies probably between the two extremes: A gate will open far enough to lower the barrier to the point where the ligand can pass. For simplicity, we take the residual barrier height to be zero in the present paper. A question then arises: Is the model "soft" so that nearly any choice of model and parameters will fit the data or is it "hard" and meaningful? To answer the question, consider Mb–O_2. We have measured rebinding after photodissociation at more than 10 temperatures in six different solvents over 9 orders of magnitude in time with more than 10 data points per decade. We observe three different processes at most temperaures; the characterization of each process requires at least two parameters (intensity and rate coefficient) at a given temperature in a given solvent. A phenomenological description of the data therefore requires $10 \times 6 \times 3 \times 2 = 360$ independent parameters. Arrhenius relations connect data at different temperatures and reduce the number of parameters ($H_{ij}^\ddagger$ and $S_{ij}^\ddagger$) to 12 in each solvent or to 52 in all solvents (assuming the innermost barrier to be unaffected by the solvent). With the model introduced under A Dynamic Model, we need only 16 parameters (12 given in Table III for Mb–O_2 and 4 for the innermost barrier) to fit the entire set of data. The model thus uses a small number of parameters to fully describe a very complex situation.

Single-Solvent Data. What can be deduced about the dynamic properties of the gates inside a protein if measurements are confined to a single solvent? To answer this question, we use eq 10 with the simplifying assumption $A_{ij}^0 \ll A_{ij}/\eta^\kappa$. For a given solvent we write again[3] $\eta = \eta_0 \exp[E_\eta/RT]$ and thus find for the rate coefficient *in a given solvent*

$$k_{ij}(T;\text{solv}) = (A_{ij}/\eta_0^{\kappa_{ij}}) \exp[-(H_{ij}^r + \kappa_{ij}E_\eta)/RT]$$

This relation has the form of a standard Arrhenius equation, but with activation energy $H_{ij}^r + \kappa E_\eta$ and not H_{ij}^r or $H_{ij}^r + E_\eta$. It is therefore not possible to extract protein parameters (H_{ij}^r, κ, and A_{ij}) from experiments with a single solvent.

Outlook. We propose in the present paper that the temperature dependence of a reaction, whether studied by flash photolysis, stopped-flow, or relaxation (T-jump) experiments, will yield information only about the protein–solvent system and not the protein alone if the measurements are performed in only one solvent. This remark is important if the data are to be compared with a model or theory, because the one-solvent approach may yield misleading results (see sections concerning Comparison with Model Calculations and Single-Solvent Data). We therefore assert that most kinetic experiments with biomolecules should be executed in a wide range of solvents and all data be interpreted together.

The data on binding of CO and O_2 to Mb (see A Dynamic Model) suggest that the barriers are dynamic and not static. All observed rates can be described with a simple model (Figure 9) in which the internal barriers are gates that open and close. Open and closed states can be identified with conformational substates, and we thus find a satisfactory answer to the question posed under Dynamic Barriers in Proteins. The transitions are governed by the rate of opening, and this rate in turn is controlled by the solvent. Control by the solvent may have implications for biological function. A change in viscosity, caused for instance by the motion of a protein from one environment to another, by attachment to a membrane, or by the binding of an effector, may influence a protein reaction. The model also supports the idea that solvent fluctuations drive protein reactions.

The discussion under A Dynamic Model also suggests that the protein is not a rigid system in which a ligand moves in a fixed potential. Rather there is a strong mutual interaction between ligand and protein, and the protein reacts to the migrating molecule.[4] CO and O_2 affect Mb differently.

The data, evaluation, and model in the present paper form only a beginning. The postulate that protein properties can be isolated by keeping the macroscopic solvent viscosity constant will have to be checked. It will be necessary to extend the measurements to other systems and solvents, check the detailed dependence on other variables such as ionic strength, compare the results with model calculations of the type performed by Karplus and collaborators, and understand more clearly the properties of the internal and external degrees of freedom of the protein (Prigogine, 1957; Lifshitz et al., 1978). In addition, the validity and form of the reaction rate equation will have to be checked at high frequencies and viscosities. Computations of the type performed by Skinner & Wolynes (1978), Chandler and co-workers (Montgomery et al., 1979), and Karplus and co-workers (Levy et al., 1979) may provide the necessary information. The identification of the various barriers with specific sites within the protein and elucidation of the mechanism of controlling the gates are two more open problems. Mobile defects proposed by Lumry & Rosenberg (1975) and Richards (1979) may account for the fluctuations that lead from the closed to the open substates.

Acknowledgments

This paper involves some unconventional ideas, and we therefore tested them, with various degrees of success, in discussions with many friends. We should like to thank all those who patiently listened, often disagreed, but always helped by suggesting improvements and new viewpoints: F. Bassani, D. Chandler, P. Douzou, H. G. Drickamer, M. Eigen, B. Gavish, V. I. Goldanskii, E. Gratton, I. C. Gunsalus, P. Hänggi, J. J. Hopfield, M. Karplus, D. Lazarus, P. Mazur, I. Prigogine, J. Turner, G. C. Wagner, M. Weissmann, and P. Wolynes.

[4] A protein is not like a solid house into which the visitor (the ligand) enters by opening doors without changing the structure. Rather it is like a tent into which a cow strays.

References

Ackerman, E., & Berger, R. L. (1963) *Biophys. J. 3*, 493.
Alben, J. O., Beece, D., Bowne, S. F., Eisenstein, L., Frauenfelder, H., Good, D., Marden, M. C., Moh, P. P., Reinisch, L., Reynolds, A. H., & Yue, K. T. (1980) *Phys. Rev. Lett. 44*, 1157.
Alberding, N., Austin, R. H., Chan, S. S., Eisenstein, L., Frauenfelder, H., Gunsalus, I. C., & Nordlund, T. M. (1976) *J. Chem. Phys. 65*, 4701.
Alberding, N., Chan, S. S., Eisenstein, L., Frauenfelder, H., Good, D., Gunsalus, I. C., Nordlund, T. M., Perutz, M. F., Reynolds, A. H., & Sorensen, L. B. (1978a) *Biochemistry 17*, 43.
Alberding, N., Frauenfelder, H., & Hänggi, P. (1978b) *Proc. Natl. Acad. Sci. U.S.A. 75*, 26.
Alpert, B., Banerjee, R., & Lindquist, L. (1974) *Proc. Natl. Acad. Sci. U.S.A. 71*, 558.
Alpert, B., El Mohsni, S., Lindquist, L., & Tfibel, F. (1979) *Chem. Phys. Lett. 64*, 11.
Austin, R. H., & Chan, S. S. (1978) *Biophys. J. 24*, 175.
Austin, R. H., Beeson, K. W., Eisenstein, L., Frauenfelder, H., & Gunsalus, I. C. (1975) *Biochemistry 14*, 5355.
Austin, R. H., Beeson, K. W., Chan, S. S., Debrunner, P. G., Downing, R., Eisenstein, L., Frauenfelder, H., & Nordlund, T. M. (1976) *Rev. Sci. Instrum. 47*, 445.
Beece, D., Eisenstein, L., Frauenfelder, H., Good, D., Marden, M. C., Reinisch, L., Reynolds, A. H., Sorensen, L. B., & Yue, K. T. (1979) *Biochemistry 18*, 3421.
Beece, D., Bowne, S. F., Czêgê, J., Eisenstein, L., Frauenfelder, H., Good, D., Marden, M. C., Marque, J., Ormos, P., Reinisch, L., & Yue, K. T. (1980) *Photochem. Photobiol.* (in press).
Brinkman, H. C. (1956) *Physica (Amsterdam) 22*, 149.
Bullock, A., Cameron, G. G., & Smith, P. M. (1974) *J. Chem. Soc., Faraday Trans. 2 70*, 1202.
Careri, G. (1974) in *Quantum Statistical Mechanics in the Natural Sciences* (Kursunoglu, B., Mintz, S. L., & Widmayer, S. M., Eds.) p 15, Plenum, New York, NY.
Careri, G., Fasella, P., & Gratton, E. (1975) *CRC Crit. Rev. Biochem. 3*, 141.
Case, D. A., & Karplus, M. (1979) *J. Mol. Biol. 132*, 343.
Chandrasekhar, S. (1943) *Rev. Mod. Phys. 15*, 1.
Cooper, A. (1976) *Proc. Natl. Acad. Sci. U.S.A. 73*, 2740.
Curme, G. O., Ed. (1952) *Glycols*, Reinhold, New York.
Douzou, P. (1977) *Cryobiochemistry*, Academic Press, London.
Frauenfelder, H. (1978) *Methods Enzymol. 54*, 506.
Frauenfelder, H. (1979) in *Tunneling in Biological Systems* (Chance, B., et al., Eds.) p 627, Academic Press, New York, NY.
Frauenfelder, H., Petsko, G., & Tsernoglou, D. (1979) *Nature (London) 280*, 558.
Gavish, B. (1978) *Biophys. Struct. Mech. 4*, 37.
Gavish, B. (1980) *Phys. Rev. Lett. 44*, 1160.
Gavish, B., & Werber, M. M. (1979) *Biochemistry 18*, 1269.
Gurd, F. R. N., & Rothgeb, T. M. (1979) *Adv. Protein Chem. 33*, 73.
Herskovits, T. T., Gadegbeku, B., & Jaillet, H. (1970) *J. Biol. Chem. 245*, 2588.
Hill, T. L. (1976) *Proc. Natl. Acad. Sci. U.S.A. 73*, 679.
Imry, Y., & Gavish, B. (1974) *J. Chem. Phys. 61*, 1554.
Ishioka, S. (1980) *J. Phys. Soc. Jpn. 48*, 367.

Keller, H., & Debrunner, P. G. (1980) *Phys. Rev. Lett. 45*, 68.
Koshland, D. (1958) *Proc. Natl. Acad. Sci. U.S.A. 44*, 98.
Kramers, H. A. (1940) *Physica (Amsterdam) 7*, 284.
Landauer, R., & Swanson, J. A. (1961) *Phys. Rev. 121*, 1668.
Larson, R. S., & Kostin, M. D. (1978) *J. Chem. Phys. 69*, 4821.
Levy, R., Karplus, M., & McCammon, J. A. (1979) *Chem. Phys. Lett. 65*, 4.
Lifshitz, I. M., Grosberg, A. Y., & Khokhlov, A. R. (1978) *Rev. Mod. Phys. 50*, 638.
Lumry, R., & Rosenberg, A. (1975) *Colloq. Int. C.N.R.S. 246*, 53.
McCammon, J. A., & Wolynes, P. G. (1977) *J. Chem. Phys. 66*, 1452.
McCammon, J. A., & Karplus, M. (1980) *CRC Crit. Rev. Biochem.* (in press).
Miner, C. S., & Dalton, N. N., Eds. (1953) *Glycerol*, Reinhold, New York.
Montgomery, J. A., Chandler, D., & Berne, B. J. (1979) *J. Chem. Phys. 70*, 4056.
Parak, F., Frolov, E. N., Mössbauer, R. L., & Goldanskii, V. I. (1980) *J. Mol. Biol.* (in press).
Prigogine, I. (1957) *The Molecular Theory of Solutions*, Interscience, New York.
Richards, F. M. (1979) *Carlsberg Res. Commun. 44*, 47.
Seidell, D. (1940) *Solubilities*, Vol. I, Van Nostrand, New York.
Sharrock, M., & Yonetani, T. (1980) *Biochim. Biophys. Acta* (in press).
Skinner, J. L., & Wolynes, P. (1978) *J. Chem. Phys. 69*, 2143.
Somogyi, B., & Damjanovich, S. (1975) *J. Theor. Biol. 48*, 393.
Weber, G. (1972) *Biochemistry 11*, 864.

Association of Alcohols with Heme Proteins: Optical Analysis and Thermodynamic Models†

Barry B. Muhoberac‡ and Arthur S. Brill*

ABSTRACT: At concentrations lower than those causing denaturation, methanol, ethanol, and 1-propanol produce changes in optical absorption of alkaline ferricytochrome *c*. These changes arise from weak equilibrium associations characterized by dissociation constants at 25 °C of about 4 and 2 M, respectively, for the methanol– and 1-propanol–ferricytochrome *c* complexes. The difference spectra and temperature dependence of enthalpy and entropy changes accompanying formation of methanol and 1-propanol complexes, as well as changes induced in the EPR spectra, are different and suggest distinct binding modes. Considered in conjunction with related parameters from ferrihemoglobin and ferrimyoglobin, the spectral and thermodynamic data are consistent with models in which methanol is bound directly to the ferric ion of cytochrome *c*, methanol and ethanol are bound directly to the ferric ions of hemoglobin and myoglobin, and 1-propanol is bound to a hydrophobic region of cytochrome *c*. Both the absolute and alcohol-induced optical difference spectra of these proteins have been simulated, the former through summation of Gaussian bands and the latter as the difference between two such summations, one with parameters slightly altered from the other. This analysis reveals and characterizes previously unresolved structure, which is discussed in terms of electronic transitions of the heme group and changes caused by differing interactions of the heme with surroundings. Similarity between the difference spectra produced by IHP perturbation of ferrihemoglobin and that from the difference between absolute spectra of ferrimyoglobin and ferrihemoglobin suggests that, with ferrihemoglobin as reference, the conformations about the hemes of ferrimyoglobin and of ferrihemoglobin–IHP are in some way similar.

Methanol and ethanol at low concentrations react with ferric myoglobin and hemoglobin to form thermodynamically and spectroscopically well-defined complexes (Brill et al., 1976). There is a similarly well-defined complex of bacterial catalase with methanol, but the binding is much weaker. The site and nature of the association of the alcohol molecules with these high-spin ferric heme proteins have not been established, and analogous studies of reactions of small alcohols with low-spin ferric heme proteins have not been reported. In this paper we describe both new experimental results and an analysis of the data at hand which contribute information about contrasting responses to the formation of complexes by proteins.

The new data reported here are from ferricytochrome *c* in alkaline solution at moderately high ionic strength. This system was chosen to allow correlation of optical and EPR[1] results. In EPR investigation of the effects of alcohols, pH, and ionic strength, there were found, for example, methanol-induced transformations in cytochrome *c* above pH 10 (see below). The use of 0.3 M NaCl makes ionic strength essentially independent of changing contributions of buffer ions when pH is varied. It should also be noted that cytochrome *c* at neutral pH has a tendency to polymerize in the presence

† From the Department of Physics and the Biophysics Program, University of Virginia, Charlottesville, Virginia 22901. *Received February 20, 1980.* This research was supported by grants from the National Heart and Lung Institute, U.S. Public Health Service (HL-13989), and the National Science Foundation (PCM76-83841).

‡ Present address: Department of Biochemistry, The University of Texas Health Science Center at San Antonio, San Antonio, TX 78284.

[1] Abbreviations used: EPR, electron paramagnetic resonance; IR, infrared; UV, ultraviolet; MCD, magnetic circular dichroism; IHP, inositol hexaphosphate.

0006-2960/80/0419-5157$01.00/0